# Analytical Methods

Accepted Manuscript


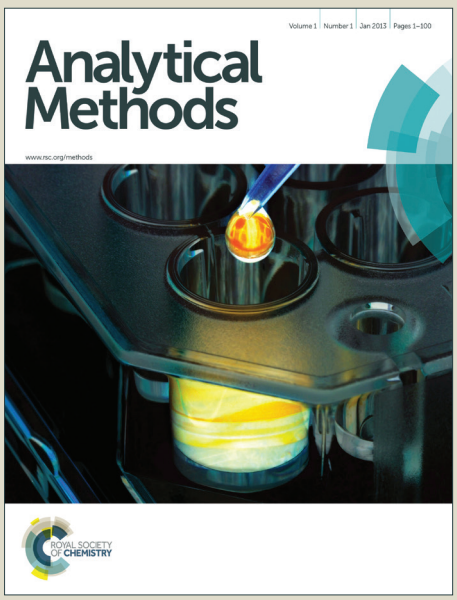





ROYAL SOCIETY OF CHEMISTRY

www.rsc.org/methods

Analytical Methods

PAPER

# Investigation on kinetic processes of zeolitic imidazolate framework-8 film growth and adsorption to chlorohydrocarbons by a quartz crystal microbalance

Dazhong Shen*, Xiaolong Ma, Tingting Cai, Xilei Zhu, Xiaodong Xin, Qi Kang

In this work, the kinetic processes of zeolitic imidazolate framework-8 (ZIF-8) film growth and the adsorption of dichloromethane (DCM), trichloromethane (TCM) and carbon tetrachloride (CTC) on ZIF-8 film were monitored in real time by a quartz crystal microbalance sensor. It was shown that the growth kinetics of ZIF-8 film from the mixture of zinc nitrate and 2-methylimidazole consists of a rapid initial growth (0.22~1.1 $\mu g.cm^{-2}.min^{-1}$) and a later slow rearrangement stages. The time to obtain 50% of total equilibrium grown mass is in the range of 5.1~6.8 min. The mass deposited in the second, third and forth cycles is 2.37, 3.36 and 4.08 times of that in the first one (3.11 $\mu g/cm^2$), respectively, and approaches to stable level after the forth cycle. The as-prepared ZIF-8 film (0.70 μm) exhibits the adsorption capacities of 568.3, 496.7 and 212.8 mg/g to DCM, TCM and TCT (20°C), respectively. The initial adsorption rate of DCM is much larger than that of TCM and CTC. The difference in the adsorption behavior of the three chlorohydrocarbons is ascribed to the sieve effect of the pore apertures in ZIF-8 to the adsorbates. The adsorption kinetic data are in agreement with the pseudo-second-order model. For the adsorption in ZIF-8 film, the adsorption activation energies are 34.9±5.6, 49.1±3.8 and 66.9±5.5 kJ/mol, the standard enthalpy changes of -63.2, -89.1 and -119 J/mol, and standard entropy changes of -41.9, -45.3, and -50.1 $kJ.mol^{-1}.K^{-1}$ have been evaluated for DCM, TCM and CTC respectively. The adsorption isotherms of DCM and TCM at 20°C are fitted well by the Langmuir model while those of CTC and TCM at 60°C follow the Freundlich model.

Received 00th January 20xx,
Accepted 00th January 20xx

DOI: 10.1039/x0xx00000x

www.rsc.org/

## 1. Introduction

Metal-organic frameworks (MOFs), a particular class of ordered porous solids, have attracted much attention in the potential applications in strategic domains such as catalysis,[1] biomedicine,[2] separation,[3] gas storage,[4] chemical sensing,[5] air purification,[6] imaging agents,[7] and so on. Among the reported MOFs, zeolitic imidazolate frameworks (ZIFs) are a sub-class of MOFs, comprising hybrid organic–inorganic moieties and exhibiting regular crystalline lattices with well-defined pore structures.[8,9] They have permanent porosity and relatively high thermal and chemical stability, which make them attractive candidates for many industrial applications. In recent years, significant progress has been made in developing ZIFs into membranes and thin films for gas separation, liquid separation and functional devices.[10] ZIF-8, as a prototypical ZIF, is formed by combining a $Zn^{2+}$ source and 2-methylimidazole (mIM) in a suitable solvent and crystallizes in a sodalite-type structure.[11] Several methods have been employed to synthesize ZIF-8 films.[12-18] On the other hand,ZIF-8 films have been applied in sensors,[19, 20] adsorbent,[21-26] catalysis,[27] capillary microreactor,[28] microelectronics,[29] and so on. Various techniques, such as in situ atomic force microscopy,[30] in situ small-angle and wide-angle X-ray scattering,[31] FTIR spectroscopy,[32] Monte Carlo simulation,[33] Raman spectroscopy,[34] inverse gas chromatography,[35] were employed to characterize the growth and adsorption of ZIF-8 film.

Quartz crystal microbalance (QCM) sensor is a useful tool for detection the mass change at the sensing surface in real time.[36-43] Recently, QCM has been applied to measure the mass change related to MOFs films.[44-54] However, growth process of MOF film, the change in viscoelasticity of the MOF film during growth and adsorption processes, the adsorption and desorption kinetics have not been well investigated. In the present study, QCM sensors were employed to monitor the growth process of ZIF-8 film from the mixture of zinc nitrate and 2-methylimidazole (mIM) in methanol and the adsorption kinetics of volatile organic compounds (VOCs). Dichloromethane (DCM), trichloromethane (TCM) and carbon tetrachloride (CTC) were chosen as the model VOCs because they are solvents used widely in chemical industry and harmful to health. The influence of the change in contact area and viscoelasticity of the ZIF-8 film on the frequency response of the QCM was corrected by using an impedance analysis method. The thermodynamic and kinetic parameters related to the adsorption of DCM, TCM and CTC on ZIF-8 films were estimated. The difference in the adsorption behaviour of the three adsorbates was discussed by the sieve effect of the pore apertures in ZIF-8 to the adsorbates.

## 2. Experimental section

### 2.1 Chemicals and materials

AT-cut 5 MHz piezoelectric quartz crystals with 14 mm wafer diameter (Model JA5, Beijing Chenjing Electronics Co., Ltd., China) were used. Two gold electrodes (key-hole configuration, geometric area = 0.407 $cm^2$) were deposited on both sides of the quartz wafer. All chemicals used were of analytical grade. The purified water used in the experiments was ion-exchanged with a Milli-Q system (Millipore, Bedford, MA, USA). Zinc nitrate and 2-methylimidazole were purchased from Shanghai Aladdin Reagents Company (China). Methanol, DCM, TCM and CTC were purchased from Tianjin Wenda Chemicals Company (China).

### 2.2 Growth of ZIF-8 film on surface of QCM plate

Before film growth, the surfaces of QCM were washed with acetone and dried by passage a stream of nitrogen. The QCM plate was mounted perpendicularly in a cell by two O-rings. 20 mL methanol was added in the cell with the height of liquid 5 mm above the top of quartz wafer. The resonant frequency ($F$) and motional resistance ($R_q$) of the QCM were measured by an impedance analyzer (4294A, Agilent) by scanning 401 frequency points in 3.7 s. When a stable baseline was achieved, half of the solvent was replaced by a freshly prepared methanolic solution of $Zn^{2+}$ and mIM. The changes in resonant frequency ($\Delta F$) and motional resistance ($\Delta R_q$) were recorded for film growth kinetics analysis. The absorbance spectra of the reaction mixture during the film growth were recorded by a spectrophotometer (UV-1700, Shimadzu Co.).

Afterwards, the QCM and the cell were washed by methanol and next growth cycle was started. Eventually, the QCM with ZiF-8 film was washed by methanol and dried at 150 °C for 2h. The X-ray powder diffraction (XRD) pattern of a typical ZIF-8 film was measured on a Bruker D8 Advance diffractometer (reflection mode, Cu $K_\alpha$ radiation λ = 1.5405 Å). The images of ZIF-8 film were taken on a scanning electron microscopy (H-800, Hitachi). Fig.1 shows the powder XRD patterns of ZIF-8 powder grown from the mixture of $Zn^{2+}$ and mIM in methanol. The peaks reveal the presence of ZIF-8 crystal under the deposition condition used in this work. The insert shows the scanning electron micrograph of the film prepared, indicating that the particles size in the film is in the range of 0.1~0.4 μm.

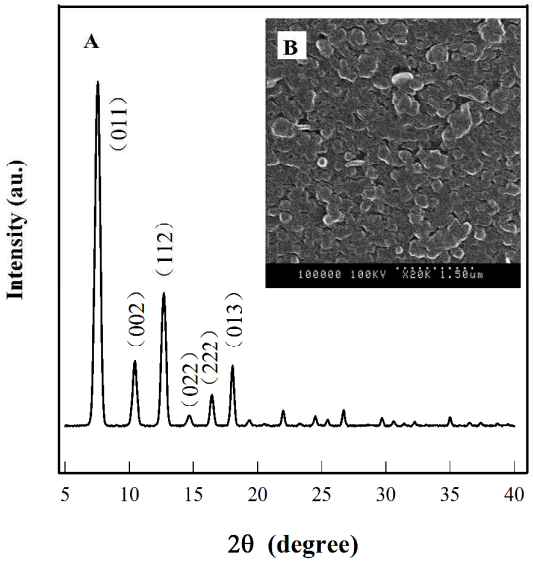


**Fig. 1** Powder XRD patterns of as-prepared ZIF-8 crystal (A) and scanning electron micrographs of the surface of the as-synthesized ZIF-8 film (B).

### 2.3 Monitor adsorption kinetic processes of chlorohydrocarbons onto ZIF-8 film

In the adsorption experiment, ZIF-8 film was grown on both sides of QCM by immersing the QCM plate in a methanolic solution of $Zn^{2+}$ and mIM. The thickness of the film was controlled by the number of growth cycle and calculated by the frequency shift of QCM measured in gaseous phase. Fig.2 shows the configuration of the experimental setup for adsorption of VOCs. A QCM with ZIF-8 film was mounted in the center of the cell. The temperature of the cell was controlled by a thermostatic bath. Prior to adsorption, the cell was vacuumized until a stable baseline of the QCM was reached. A given volume of VOCs (DCM, TCM or CTC) was injected into the cell by a microsyringe. The solvent was vaporized rapidly in the cell and the adsorption process was started. A magnetic mixer was used to speed up the diffusion of the solvent vapour. The responses of QCM ($\Delta F$ and $\Delta R_q$) were recorded to estimate the mass adsorbed and adsorption kinetic parameters. After an adsorption procedure, the cell was exhausted by a vacuum pump to regenerate the ZIF-8 film for next adsorption.

All the adsorption experiments were performed thrice and the averaged values were reported.

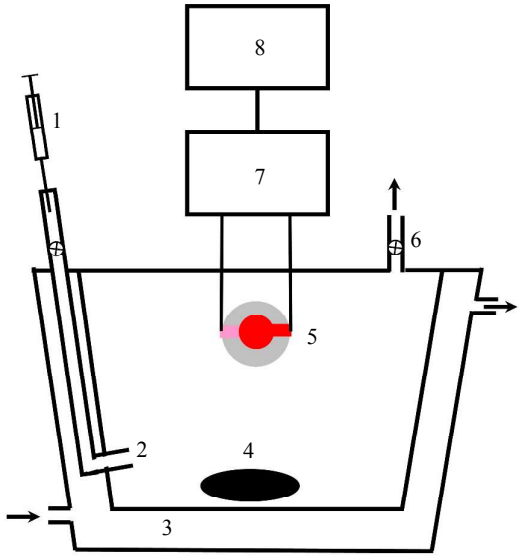


**Fig. 2** Schematic drawing of experimental setup employed for the adsorption measurements (not to scale). (1): syringe with organic solvent; (2): inlet for adsorbate vapor; (3): thermostatic water bath; (4): magnetic mixer; (5): QCM sensor with ZIF-8 film; (6): vacuum pump; (7): impedance analyzer; (8): computer.

## 3. Results and discussion

### 3.1 Response of QCM in growth process of ZIF-8 film

In this experiment, the growth process of ZIF-8 film was monitored by the frequency shift of the QCM sensor in real time. As shown in Fig.3, the frequency of QCM decreases after adding a freshly prepared methanolic solution of mIM and $Zn^{2+}$, suggesting the growth of ZIF-8 film on the surface of the QCM plate. Usually, the mass change is calculated from the frequency shift of QCM according to Sauerbrey equation in Eq. (1). [36]

$$\Delta F = -2.26\times10^{-6} f_0^2 \frac{\Delta m}{A_e} \quad (1)$$

where $f_0$ and $A_c$ the fundamental frequency and the electrode area of the quartz resonator, respectively.

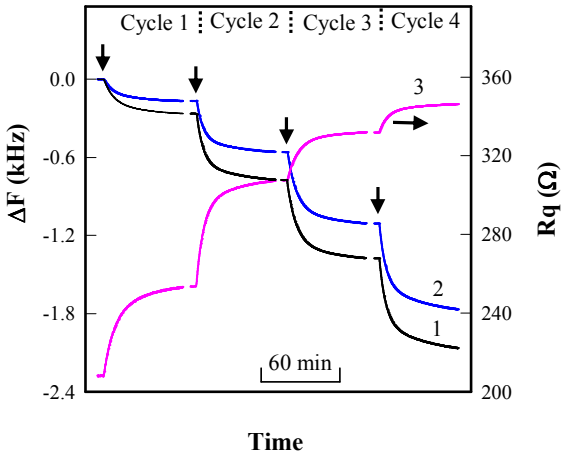


**Fig. 3** Changes in frequency and motional resistance of QCM during the processes of growth ZIF-8 films. The arrow indicates the start of a new fabrication cycle by addition of fresh mixture of 25 mM $Zn^{2+}$ and 50 mM mIm in the cell. (1): measured frequency shift (black); (2): corrected frequency shift (blue); (3): motional resistance (pink).

It should be noted that the Sauerbrey equation is valid only for an ultrathin, homogeneous and rigid mass loading on the surface of the electrodes of the QCM. For a QCM operating in a liquid phase, its frequency response is related to the changes in both of surface mass loading and the liquid properties.[39] As shown in Fig.3, the decreased frequency is companied by an increased motional resistance in a similar rate, indicating a larger energy loss from the oscillating QCM surface to the liquid phase. According to Muramatsu et al, [55] the motional resistance of the QCM is expressed by.

$$R_q = \frac{A\left(2\pi f_0 \eta \rho\right)^{1/2}}{K^2} \qquad (2)$$

where A is the contact area between the electrode and the liquid, η and ρ are the viscosity and density of the liquid phase, K is the electromechanical coupling factor of the quartz, respectively.

However，in a separated experiment, near constant values of η and ρ of the reaction mixture were measured during the fabrication processes of ZIF-8 films. Hence, the increased $R_q$ is attributed to an increased surface roughness of the electrode after ZIF-8 film deposition. With increasing film thickness, the contact area of the film with liquid is expected to increase, resulting in a larger energy loss from QCM plate to the liquid phase. On the other hand, a liquid layer attached to the oscillating QCM plate is equivalent to an additional mass loading for the QCM. According to Kanazawa and Gordon,[56] the frequency of the QCM in contact with a fluid decreases linearly with increasing $(\eta\rho)^{1/2}$. With increasing surface roughness, the absolute value of the slope in the plotting of frequency versus $(\eta\rho)^{1/2}$ increases.[57] To account for the influence of the surface roughness on the response of QCM in viscous model, we add a coefficient in the relation derived by Kanazawa and Gordon.

$$\Delta F_{\text{liquid}} = -\gamma f_0^{3/2}\left(\frac{\rho\eta}{\pi\mu_q\rho_q}\right)^{1/2} \qquad (3)$$

where $\Delta F_{\text{liquid}}$ is the frequency shift due to the additional mass loading from the liquid layer, $\mu_q$ and $\rho_q$ are the elastic modulus and the density of the quartz, $\gamma$ is the ratio of the contact area between ZIF-8 film and the liquid to its geometrical area, respectively.

In the case of a homogeneous film, there is $A = \gamma A_e$ in Eq.(2). Hence, it is reasonable to estimate the value of $\Delta F_{\text{liquid}}$ indirectly from $\Delta R_q$ based on correlation between $\Delta R_q$ and $\Delta F_{\text{liquid}}$ in Eq.(2) and (3).

$$\Delta F_{\text{liquid}} = -\frac{\gamma f_0 K^2}{A_e \pi (2\mu_q\rho_q)^{1/2}}\Delta R_q = \alpha \Delta R_q \qquad (4)$$

It can be seen that the coefficient of α is independent to the properties of solution and the surface roughness of the film coated. Based on the values of $\Delta R_q$ and $\Delta F_{\text{liquid}}$ measured in a group of glycerol aqueous solutions in concentration range of 0 to 50%, the value of α = –2.157 Hz/Ω was obtained for the estimation of $\Delta F_{\text{liquid}}$. For example, $R_q$ is increased from 208 Ω to 346 Ω in Fig.3 after four growth cycles, corresponding to $\Delta F_{\text{liquid}}$ = –988 Hz based on Eq.(4) due to the increased contact area. The value of $\Delta F_{\text{liquid}}$ is 14.4% of the total frequency shift. After deducting the contribution from $\Delta F_{\text{liquid}}$, the corrected frequency shift (–1767 Hz) is close to the value of $\Delta F$ = –1683 Hz measured in gaseous phase after vacuum dry. The difference in frequency shift may be due to the adsorption of methanol onto ZIF-8 film in liquid phase. Hence, the corrected frequency shift, $\Delta F_0 = \Delta F - \Delta F_{\text{liquid}}$, was used to monitor the mass of ZIF-8 film grown in the fabrication processes. The film thickness ($h$) is calculated by:

$$h = \frac{m_f}{A_e\rho_f} = -\frac{4.43\times10^5(\Delta F - \alpha\Delta R_q)}{\rho_f f_0^2} \qquad (5)$$

where $m_f$ and $\rho_f$ (=0.95g/cm$^3$) are the mass of film grown and density of ZIF-8 film, [58] respectively.

### 3.2 Kinetic characteristics in ZIF-8 film growth processes

By using the corrected frequency shift, the growth rate of ZIF-8 film can be monitored by a QCM in real time. As shown in Fig.3, the growth rate is relatively high in the initial stage in each growth cycle and decays with the growth time. In all the growth cycles, the relations between $\Delta m_f$ and growth time ($t$) are well fitted by the following five parameters exponential decay model.

$$\Delta m_f = m_0 - m_1 e^{-r_1 t} - m_2 e^{-r_2 t} \qquad (6)$$

where $m_0$ ($\approx m_1 + m_2$) is the total equilibrium mass grown in a growth cycle, $m_1$ and $m_2$ the equilibrium mass corresponding to the rapid initial growth and later slow rearrangement stages, $r_1$ and $r_2$ ($r_1 > r_2$) the observed growth rate constants, respectively.

Yamamoto and co-worker synthesized size-controlled ZIF-8 nanoparticles using a T-type micromixer, indicating the synthetic mechanism involves a nucleation process and a particle growth process.[59] In the fresh mixture of $Zn^{2+}$ and mIM, the concentration of fine ZIF-8 crystallite in solution is relatively high, resulting in a rapid growth stage. With increasing reaction time, larger crystallites are expected to grow while the smaller crystallites are dissolved due to the dependence of solubility on the size of crystallites. Hence, a slow rearrangement stages is observed in Fig.3. For example, the growth of ZIF-8 film is observable even after 60 min. This analysis is supported by the absorbance spectra in Fig.4. In a freshly prepared

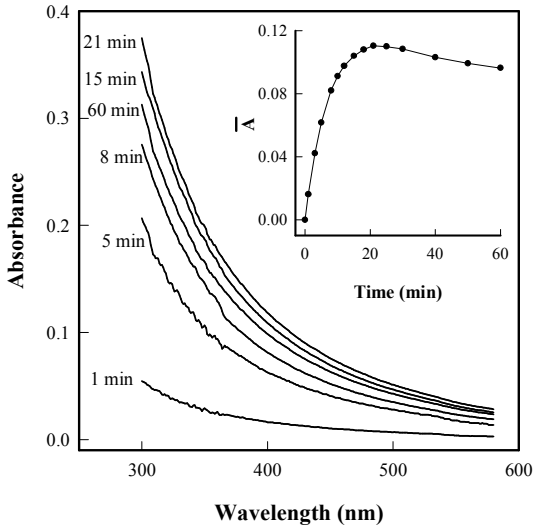


**Fig. 4** Changes in absorbance spectrum of the reaction mixture during the processes of growth ZIF-8 films. Insert: Change of the averaged absorbance with the reaction time.

methanolic solution of mIM and $Zn(NO_3)_2$, the ZIF-8 nanoparticles size is very small. As a result, the absorbance (with wavelength > 300 nm) is low because the absorbance spectra of mIM and $Zn(NO_3)_2$ are not in this region. With increasing reaction time, the size of ZIF-8 crystallite increases, indicating by the increased absorbance. The increased absorbance is ascribed to the light scattering effect from the crystallite of ZIF-8 in solution as well as the absorbance of ZIF-8 film on the wall. It is well known that the intensity of scattering increases remarkably with increasing diameter of the particles and decreases significantly with increasing wavelength. As shown in the inset in Fig.4, the averaged absorbance in the wavelength region ( $\overline{A}$ ) increases near-linearly in the initial 10 min and reached a maximum at 21 min then decreases slightly. The decreased absorbance is caused by the sedimentation of larger ZIF-8 crystallites.

Table 1 lists the regressed parameters in Eq.(6). Under our experimental conditions, the value of $m_0$ in the first growth cycle (3.11 μg/cm$^2$) is the smallest with ZIF-8 grown on Au surface. Afterward, the ZIF-8 layer in the previous growth cycle is used as the seed for film growth. Hence, the mass and rate in the subsequent cycles are increased. The values of $m_0$ in the second, third and forth cycles are 2.37, 3.36 and 4.08 times of that in the first one, respectively, and approaches to a stable level after the forth cycle. The reason for the increase in $m_0$ may be ascribed to the increase in the contact area of the ZIF-8 film on the surface of QCM to solution, which is helpful for the growth of ZIF-8 crystallites. As discussed above, the increase in $R_q$ is corresponded to the increase in contact area of the ZIF-8 film on QCM plate. As shown in Fig.3, the value of $R_q$ is increased obviously in the first and second growth cycles and approached stable level with increasing growth cycle, which is in agreement with the change trend in $m_0$. In addition, the observed rate constants of $r_1$ are in the range of 0.158~0.221 min$^{-1}$. The times to obtain 50% of total equilibrium growth mass, $t_{0.5}$, are in the range of 5.1~6.8 min. The averaged deposition rate of film in the initial

**Table 1** Regressed parameters in Eq.(6) for ZIF-8 film fabrication in different growth cycles

| growth cycle | $m_0$ μg/cm$^2$ | $m_1$ μg/cm$^2$ | $r_1$ min$^{-1}$ | $m_2$ μg/cm$^2$ | $r_2$ min$^{-1}$ | $t_{0.5}$ min |
|---|---|---|---|---|---|---|
| 1 | 3.11 | 1.78 | 0.163 | 1.34 | 0.0336 | 6.8 |
| 2 | 7.37 | 5.26 | 0.221 | 2.27 | 0.0277 | 5.1 |
| 3 | 10.47 | 7.90 | 0.158 | 2.68 | 0.0209 | 6.7 |
| 4 | 12.68 | 8.27 | 0.208 | 4.36 | 0.0253 | 5.8 |
| 5 | 12.51 | 8.45 | 0.216 | 4.13 | 0.0239 | 5.3 |

growth stage (0~ $t_{0.5}$) increased from 0.218 μg.cm$^{-2}$.min$^{-1}$ in the first growth cycle to 1.10 μg.cm$^{-2}$.min$^{-1}$ in the fifth cycles.

### 3.3 Response of QCM in the adsorption kinetic process of DCM on ZIF-8 film

With DCM as the model adsorbate, the adsorption kinetic process on ZIF-8 film was monitored from the response of the QCM. Under the initial low pressure condition, DCE is vaporized immediately and diffuses to the surface of ZIF-8 film. As shown in Fig.5, the frequency of the QCM decreases after injecting of DCM into the cell. During the adsorption process, the motional resistance of the QCM also increases slightly, indicating the increase in viscoelasticity of the film with DCM adsorbed. Hence, the mass of absorbate adsorbed ($Q$, mol/cm$^2$) is calculated according to the Sauerbrey equation by using the corrected frequency shift.

$$Q = -\frac{4.43\times10^5(\Delta F - \alpha\Delta R_q)}{Mf_0^2} \quad (7)$$

where $M$ is the molecular mass of the adsorbate.

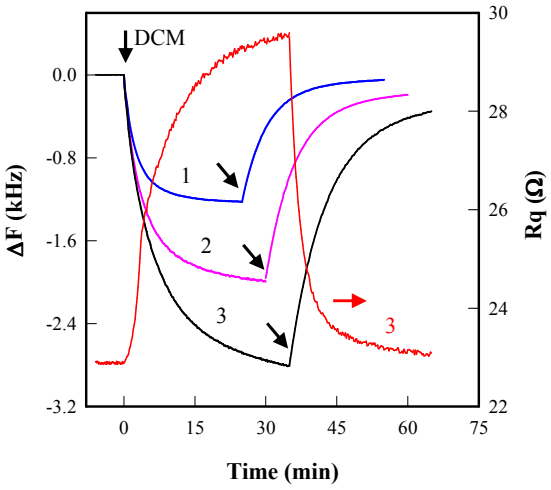


**Fig. 5** Changes of the frequency and motional resistance of QCM in the processes of the adsorption and desorption of TCM on ZIF-8 film (20°C). ZIF-8 film thickness: (1): $h$=0.36μm; (2): $h$=0.70μm; (3): $h$=1.28μm. The amount of DCM was 0.716 mmol/L. The inclined arrows indicate the start of an exhaustion process using vacuum pump.

When the cell is vacuumized, the frequency of QCM increases whiles the motional resistance decreases, suggesting the desorption took place due to the decreased DCM concentration in the cell. But the frequency does not return to previous baseline level in a short time. The reason is that some of the adsorbate molecules adsorbed in internal cavities of ZIF-8 film do not escape rapidly due to the resistance of mass transfer. If the adsorption cell is blown by nitrogen for 5 min and is vacuumized again, the desorption process is speeded up to regenerate ZIF-8 film for next adsorption operation.

As can be seen in Fig.5, with increasing film thickness, a larger frequency decrease is observed, corresponding to a higher mass adsorbed on unit area of the film (mol/cm$^2$). But the adsorption sites in the deeper layer of the film have less chance to adsorb DCM molecules. In fact, the utilization efficiency of the adsorption sites in thicker film reduces due to a larger resistance for molecule diffusion. Hence, the amount adsorbed in unit mass of film (mol/g) decreases with increasing film thickness. According to Fig.5, the amounts of DCM adsorbed at 20 min are 0.253, 0.407 and 0.558 μmol/cm$^2$ in ZIF-8 film of thickness of 0.36, 0.70 and 1.28 μm, which are 59.7%, 49.4% and 37.0% of the mass of film, respectively. On the other hand, the time to achieve adsorption equilibrium was prolonged with increasing film thickness.

### 3.4 Influence of temperature on adsorption kinetics

In this experiment, the adsorption of the three chlorohydrocarbons at 20, 40 and 60°C is compared. As shown in Fig.6, with increasing temperature, the adsorption rate is increased and the time to achieve adsorption equilibrium is shortened. The amount of CTC adsorbed is much less than that of DCM and TCM. On the other hand, the adsorption rate of TCM is obviously less than that of DCM. One reason is that the volatilization rate of a solvent reduces with increasing boiling point. The boiling points of DCM, TCM and CTC are 39.8, 61.8 and 76.8°C, respectively. At the concentration used, they are expected to volatilize completely under the condition of low pressure. The higher volatilization rate of DCM resulted in higher adsorption rate. Another reason is due to the difference in the molecular size of the adsorbates, which is discussed in the next section.

In order to investigate the adsorption kinetics, two kinetic models were used, which are pseudo-first-order and second-order models. The linear forms of the two kinetic models are expressed by. [60]

$$\ln(Q_e - Q_t) = \ln Q_e - k_1 t \quad (8)$$

$$\frac{t}{Q_t} = \frac{1}{k_2 Q_e^2} + \frac{t}{Q_e} \quad (9)$$

where $k_1$ and $k_2$ are the rate constants of pseudo-first-order and pseudo-second-order models, respectively. The reciprocal of the intercept in Eq.(9) is defined as the initial rate of adsorption ($V_0 = k_2 Q_e^2$).

Fig.7 depicts the plots of $t/Q_t$ vs. $t$ for the adsorption of the three adsorbates at different temperature. The correlation coefficients ($R^2$) are in the ranges of 0.9859~0.999, which are higher than those of 0.92-0.96 in pseudo-first-order model (data are not shown). Under the experimental conditions used, it is ascertained from a comparison of the predicted (best fitted) time dependencies with the experimental data that the pseudo-second-order kinetic equation described the adsorption processes of DCM, TCM and CTC on ZIF-8 film more accurately.

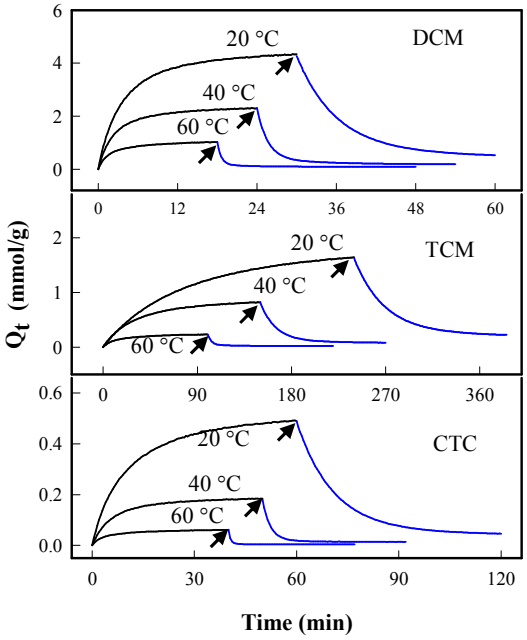


**Fig. 6** Influence of temperature on the amount adsorbed in ZIF-8 film (0.70μm) in adsorption and desorption processes. The inclined arrows indicate the start of an exhaustion process using vacuum pump. The amounts of DCM, TCM and CTC added were 0.716, 1.17 and 1.74 mmol/L, respectively.

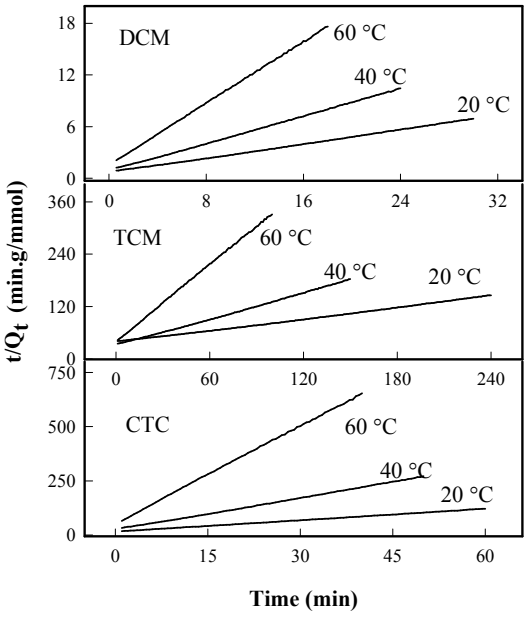


**Fig. 7** Pseudo-second-order kinetics for DCM, CTM and CTC adsorption in ZIF-8 film. The experimental conditions are the same as Fig.6.

### 3.5 Comparison of the adsorption behavior of DCM, TCM and CTC on ZIF-8 film

Fig.8 depicts the adsorption isotherms of DCM, TCM and CTC onto ZIF-8 film at different temperature. In the concentration range used in this experiment, according to the law of ideal gas, the vapour pressures of the adsorbates under low pressure conditions are less obviously than their saturation vapour pressures at the same temperature (see Electronic Supplementary Information (ESI)). Hence, the concentration of the adsorbate in the cell is assumed to be close to the amount added. In addition, the loss of adsorbate by the adsorption on the wall of cell and the film is ignored for simplification the data analysis. The isotherm data are treated according to the well-known Langmuir and Freundlich isotherm models, which are formulated as

$$Q_e = Q_{max} K_L C_e / (1 + K_L C_e) \quad (10)$$

$$Q_e = K_F C_e^{1/n} \quad (11)$$

where $Q_{max}$ (mg/g) and $K_L$ (L/g) are the saturation adsorption capacity and adsorption equilibrium constant in Langmuir model, $K_F$ and $1/n$ are Freundlich constants, respectively, $C_e$ is the equilibrium concentration of adsorbate (mg/L).

The fitting constants in the Langmuir and Freundlich models are listed in Table 2. For DCM adsorption, the Langmuir model is found to represent the equilibrium data with a much better fit as compared to the Freundlich model. The values of $Q_{max}$ and $K_L$ decrease with increasing temperature (20~60°C). For TCM adsorption at 20, 40 and 60°C, the correlation coefficients for the Langmuir isotherm model are higher, near same and less than those obtained on applying the Freundlich model, respectively. For CTC adsorption, the Freundlich model represents the isotherm data better than the Langmuir model. The Freundlich constant, 1/n, is a measure of adsorption intensity. As the value of 1/n increases, the adsorption bond becomes weaker. For adsorption of TCM and CTC at 60°C, the values of 1/n are close to 1. Hence, the amount adsorbed increases near-linearly with increasing amount added.

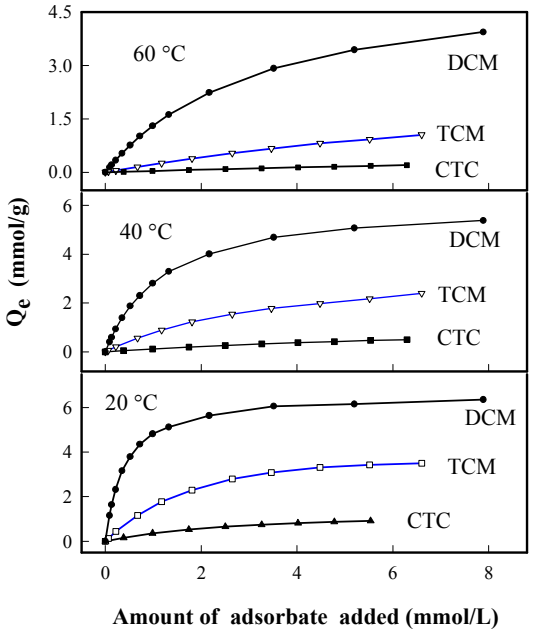


**Fig.8** Adsorption isotherms of DCM, CTM and CTC in ZIF-8 film (0.70μm) at different temperature.

**Table 2** Fitting constants and coefficients of correlation ($R^2$) for Langmuir and Freundlich equations to the experimental data for DCM，TCM and TCT adsorption on ZIF-8 films with thickness of 0.70 μm.

| VOCs | $T$ °C | Langmuir model | | | Freundlich model | | |
|---|---|---|---|---|---|---|---|
| | | $Q_{max}$ mmol/g | $K_L$ L/mol | $R^2$ | $K_F$ | $1/n$ | $R^2$ |
| DCM | 20 | 6.691 | 2565 | 0.9985 | 4.710 | 0.262 | 0.9235 |
| | 40 | 6.237 | 831.5 | 0.9943 | 2.543 | 0.415 | 0.9546 |
| | 60 | 5.549 | 310.8 | 0.9926 | 1.286 | 0.576 | 0.9785 |
| TCM | 20 | 4.160 | 507.5 | 0.9936 | 1.551 | 0.515 | 0.9857 |
| | 40 | 3.571 | 285.3 | 0.9918 | 0.799 | 0.611 | 0.9920 |
| | 60 | 3.483 | 68.29 | 0.9904 | 0.233 | 0.822 | 0.9954 |
| CTC | 20 | 1.383 | 361.5 | 0.9893 | 0.391 | 0.496 | 0.9985 |
| | 40 | 1.272 | 104.1 | 0.9858 | 0.131 | 0.734 | 0.9960 |
| | 60 | 1.089 | 35.53 | 0.9831 | 0.0395 | 0.881 | 0.9931 |

Under the experimental conditions used, ZIF-8 film exhibits high adsorption capacity to DCM and TCM. For example, the value of $Q_{max}$ for the adsorption of DCM at 20 °C is 6.691 mmol/g, which corresponds to 56.2% of the ZIF-8 film mass. The values of $Q_{max}$ and $K_L$ are in the order of DCM >TCM > CTC. On the other hand, as shown in Fig.9, the initial adsorption rate of DCM is much larger than that of TCM and CTC. The difference in the adsorption behaviour of the three chlorohydrocarbons is explained below.

ZIF-8 can be described as having a formula of $Zn(mIM)_2$ and having a sodalite-like topology with internal cavities 1.16 nm in diameter connected by windowlike pore apertures 0.34 nm across.[35,61] DCM, TCM and CTC are chlorohydrocarbons from methane with increasing numbers of C-Cl bond. According to molecular simulation calculation (see Fig.S1-1 in ESI), the bond lengths of C-H and C-Cl in DCM are 0.107 and 0.183 nm, and the bond angle between H-C-H, H-C-Cl and Cl-C-Cl are 113.3, 107.9 and 112.2 deg., respectively. By using 0.037 and 0.099 nm as the atomic radius of H and Cl in DCM, the maximum distance between H to H, H to Cl, and Cl to Cl are 0.241, 0.354 and 0.468 nm, respectively. Hence, the minimum triangle (ΔHHCl) in the tetrahedral structure of DCM is in a circle with a kinetic diameter of 0.376 nm (see Fig.S1-2 in ESI). Although this kinetic diameter exceeds the small pore aperture size of ZIF-8 (0.34 nm), DCM is expected to allow entry because the pore apertures of ZIF-8 are not circular and have some flexibility to accommodate guest molecules,[62] indicating by the high adsorption capacity. It has been reported that the cutoff for the kinetic diameter of monobranched alkanes is at or above 0.5 nm, significantly larger than the openings in the ZIF-8 structure.[63] Similarly, the diameter of the circle connected to the minimum triangle in the tetrahedral structure of TCM (ΔHClCl) is estimated to be 0.468 nm (see Fig.S2-2 in ESI).

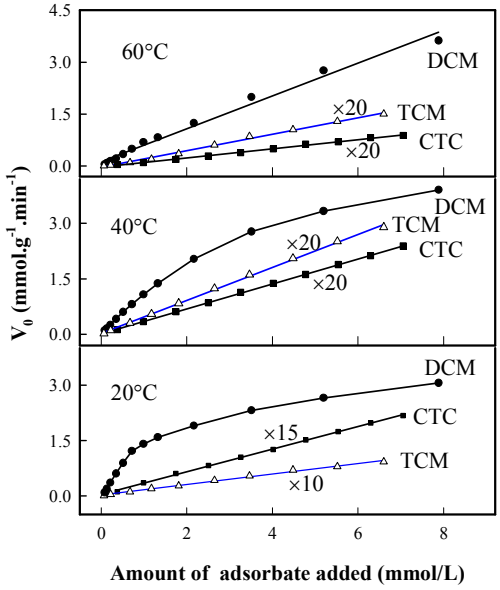


**Fig. 9** Dependence of the initial rate of adsorption on the amounts of adsorbate added and temperature.

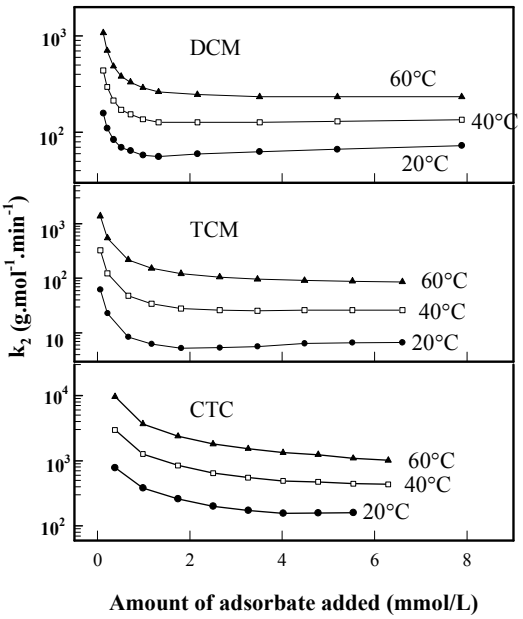


**Fig. 10** Dependence of the adsorption rate constants of the pseudo-second-order model on the amounts of adsorbate added and temperature.

The increased kinetic diameter makes it more difficult for TCM to pass through the small pore apertures of ZIF-8. Hence, the adsorption rate of TCM is remarkably less than that of DCM (Fig.9). In addition, the adsorption capacity of ZIF-8 film to TCM is also less than that to DCM. Because the minimum kinetic diameter for CTC (0.530 nm, see Fig.S3-2 in ESI) is larger than the cutoff of the pore aperture (0.5 nm), it is reasonable to assume that the adsorption of CTC on the surface of the film is preponderant because CTC has less chance to enter the internal cavities in ZIF-8 film. As a result, the amount of CTC adsorbed is reduced remarkably. On the other hand, the time to achieve adsorption equilibrium is shortened as most of CTC was adsorbed on the surface of ZIF-8 film.

### 3.6 Adsorption kinetic and thermodynamic parameters of chlorohydrocarbons on ZIF-8 film

Fig.10 shows the dependence of the rate constant in the pseudo-second-order model on temperature and the amount of adsorbate added. It can be seen that the rate constant increases with increasing temperature. In the region of low amount of adsorbate added, the rate constant reduces with increasing vapour concentration. The dependence of adsorption rate constant on temperature can be used to estimate adsorption activation energy ($E_a$) according to the Arrhenius's equation. [64]

$$\ln k = \ln A_0 - \frac{E_a}{RT} \qquad (12)$$

where $A_0$ is a constant called the frequency factor, $R$ is the universal gas constant, T is the temperature in Kelvin.

Consequently, when ln$k$ is plotted versus 1/T, a straight line with slope -E/R is obtained. Under the experimental conditions used, the values of $E_a$ are reduced with increasing amount of adsorbate added (Fig.11). The averaged values of $E_a$ are 34.9± 5.6, 49.1±3.8 and

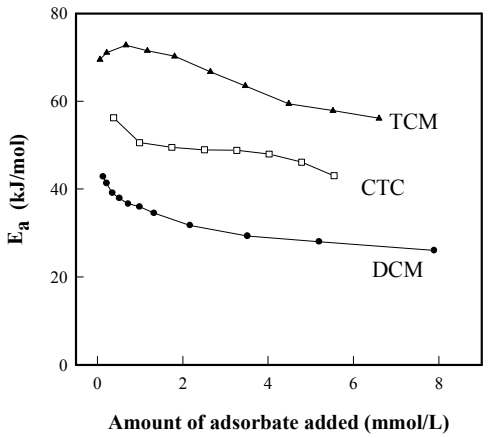


**Fig. 11** Dependence of the adsorption activation energy on the amounts of adsorbate added.

66.9± 5.5 kJ/mol for DCM, TCM and CTC, respectively. The lowest activation energy for DCM adsorption is ascribed to the smallest molecular size among the three adsorbates. But the activation energy for CTC is less than TCM. The possibility is that the adsorption of CTC on the surface of ZIF-8 film is preponderant.

The dependence of thermodynamic equilibrium constant ($K$s) on temperature can be used to estimate thermodynamic parameters, including the free energy changes ( $\Delta G^0_{ads}$ ), standard enthalpy

changes ($\Delta H^0_{ads}$) and the entropy changes ($\Delta S^0_{ads}$) associated with the adsorption process. It can be calculated by:

$$\Delta G^0_{ads} = -RT \ln K_S \quad (13)$$

$$\ln K_S = \frac{-\Delta H^0_{ads}}{RT} + \frac{\Delta S^0_{ads}}{R} \quad (14)$$

The values of $K_S$ are obtained by plotting $\ln(C_S/C_e)$ versus $C_S$ and extrapolating to $C_S$=0 as suggested by Khan and Singh.[65,66] Where $C$s is the surface concentration of adsorbate in per volume of ZIF-8 film (mg/L), calculated by using the density of 0.95 for ZIF-8 crystal [58]. The plots of $\ln K_S$ against 1/T (Fig. 12) yields straight lines, from which the values of $\Delta H^0_{ads}$ and $\Delta S^0_{ads}$ can be calculated from the slope and intercept, respectively. The results are listed in Table 3.

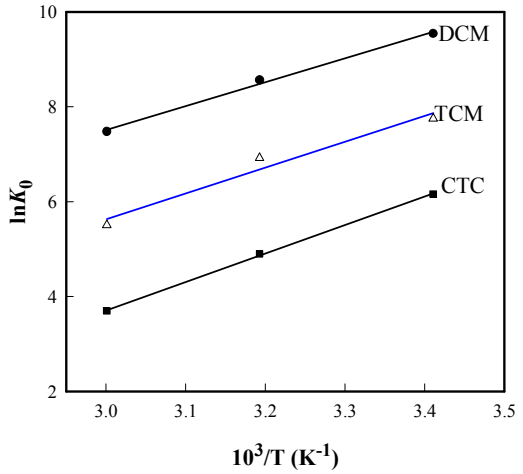


**Fig.12** Determination of adsorption enthalpy of DCM, CTM and CTC on ZIF-8 film (0.70μm).

**Table 3** Values of the thermodynamic parameters for the adsorption of DCM, TCM and CTC on ZIF-8 films with a thickness of 0.70 μm.

| VOCs | $T$ °C | $\ln K_0$ | $\Delta G^0$ kJ/mol | $\Delta H^0$ kJ/mol | $\Delta S^0$ J.K$^{-1}$.mol$^{-1}$ |
|---|---|---|---|---|---|
| DCM | 20 | 9.53 | -23.3 | -41.9 | -62.7 |
| | 40 | 8.56 | -22.3 | | |
| | 60 | 7.48 | -20.7 | | |
| TCM | 20 | 7.75 | -18.9 | -45.3 | -87.2 |
| | 40 | 6.92 | -18.0 | | |
| | 60 | 5.51 | -15.3 | | |
| CTC | 20 | 6.16 | -15.1 | -50.1 | -119.1 |
| | 40 | 4.91 | -12.8 | | |
| | 60 | 3.69 | -10.2 | | |

The Gibbs free energy changes $\Delta G^0_{ads}$ are in the range of −23.3 to −10.2 kJ/mol, which indicate that the processes are spontaneous. Moreover, the decreased $\Delta G^0_{ads}$ with increased temperature indicates the presence of an energy barrier at higher temperature in adsorption. Hence, the adsorption is less favourable at higher temperatures, which is verified by the adsorption isotherms (Fig.9). The enthalpy change $\Delta H^0_{ads}$ of the systems are negative, indicating that the adsorption of DCM, TCM and CTC onto ZIF-8 is exothermic. In addition, the negative standard entropy change $\Delta S^0_{ads}$ implies that the regular degree of the adsorption system increases due to the freedom degree of the adsorbed species decrease.

## 4. Conclusion

This work clearly demonstrates the benefits of the use of QCM in the investigation of MOFs film growth and adsorption kinetic processes. QCM experiments are typically performed with small sample quantities of just a few micrograms, allowing heat and mass transfer issues that occur with larger sample sizes to be avoided. They allow on-line and direct detection of label-free adsorbates, thus saving time and providing the opportunity to study the kinetics of the adsorption process. Under the conditions used in this work, the change in the motional resistance of QCM is observed during the growth and adsorption processes. The influence of the change in contact area and viscoelasticity of the ZIF-8 film is corrected in an impedance analysis method. The growth kinetics of ZIF-8 film consists of a rapid initial growth and a later slow rearrangement stages. The time to obtain 50% of total equilibrium growth mass is in the range of 5.1~6.8 min. The mass deposited in the second, third and forth cycles is 2.37, 3.36 and 4.08 times of that in the first one (3.11 μg/cm$^2$), respectively, and approaches to stable level after the forth cycle. The ZIF-8 film (0.70 μm) has the adsorption capacity of 568.3, 496.7 and 212.8 mg/g to DCM, TCM and TCT (20°C), respectively. The initial adsorption rate of DCM is much larger than that of TCM and CTC. The difference in the adsorption behaviour of the three chlorohydrocarbons is ascribed to the sieve effect of the pore apertures in ZIF-8 to the adsorbates. The adsorption kinetic data are found to be in agreement with the pseudo-second-order model. The adsorption activation energies are 34.9± 5.6, 49.1±3.8 and 66.9± 5.5 kJ/mol, the standard enthalpy changes of -63.2; -89.1 and -119 J/mol, and standard entropy changes of -41.9, -45.3, and -50.1 kJ.mol$^{-1}$.K$^{-1}$ have been evaluated for DCM, TCM and CTC respectively.

## Acknowledgements

The authors gratefully acknowledge financial support of National Natural Science Foundation of China (21175084, 21275091, 21575080), the Opening Fund of Key Laboratory of Chemical Biology and Traditional Chinese Medicine Research (Hunan Normal University), Ministry of Education (KLCBTCMR2011-01) and Research Fund for the Doctoral Program of Higher Education of China (No. 20113704110003).

## Notes and references

*College of Chemistry, Chemical Engineering and Materials Science, Collaborative Innovation Center of Functionalized Probes for Chemical Imaging in Universities of Shandong, Key Laboratory of*



 

*Molecular and Nano Probes, Ministry of Education, Shandong Provincial Key Laboratory of Clean Production of Fine Chemicals, Shandong Normal University, Jinan, 250014, P. R .China. Corresponding author. Tel.: +86 0531 86180740; fax: +86 053182615258. E-mail address: dzshen@sdnu.edu.cn (D. Shen).*

**Electronic Supplementary Information**

Additional information as noted in text. This material is available free of charge via the Internet at http://www.rsc.org.

1 A. Aijaz, N. Fujiwara and Q. Xu, *J. Am. Chem. Soc.*, 2014, **136**, 6790.

2 P. Horcajada, R. Gref, T. Baati, P. K. Allan, G. Maurin, P. Couvreur,G. Férey, R.E. Morris and Christian Serre, *Chem. Rev.*, 2012, **112**, 1232.

3 J. R. Li, J. Sculley and H. C. Zhou, *Chem. Rev.*, 2012, **112**, 869.

4 K. Sumida, D. L. Rogow, J. A. Mason, T. M. McDonald, E. D. Bloch, Z. R. Herm, T.H. Bae and J. R. Long, *Chem. Rev.*, 2012, **112**, 724.

5 J. P. Lei, R.C. Qian, P. H. Ling, L. Cui and H. X. Ju, *Trends in Anal. Chem.*, 2014, **58**, 71.

6 J. B. DeCoste and G. W. Peterson, *Chem. Rev.*, 2014, **114**, 5695.

7 D. Liu, K. Lu, C. Poon and W. Lin, *Inorg. Chem.*, 2014, **53**, 1916.

8 N. Stock and S. Biswas, *Chem. Rev.*, 2012,**112**, 933.

9 B. L. Chen, Z. X. Yang, Y. Q. Zhu and Y. D. Xia, *J. Mater. Chem. A*, 2014, **2**, 16811.

10 J.F. Yao and H.T. Wang, *Chem. Soc. Rev.*, 2014, **43**, 4470.

11 E. L. Bustamante, J. Fernández and J. M. Zamaro, *J. Colloid Interface Sci.*, 2014, **424**, 37.

12 S. Z. Li , W. X. Shi , G. Lu, S. Z. Li, S. C. J. Loo and F. W. Huo, *Adv. Mater.*, 2012, **24**, 5954.

13 H. T. Kwon and H. K. Jeong, *J. Am. Chem. Soc.*, 2013, **135**, 10763.

14 K. Khaletskaya, S. Turner, M. Tu, S. Wannapaiboon, A. Schneemann, R. Meyer, A. Ludwig, G. Van Tendeloo and R. A. Fischer, *Adv. Funct. Mater.*, 2014, **24**, 4804.

15 M. Shaha, H. T. Kwon, V. Tran, S. Sachdeva, H. K. Jeong, *Microporous Mesoporous Mater.*, 2013, **165**, 63.

16 K. Kida, K. Fujita, T. Shimada, S. Tanaka and Y. Miyake, *Dalton Trans.*, 2013, **42**, 11128.

17 A. M. Joaristi, J. Juan-Alcañiz, P. Serra-Crespo, F. Kapteijn and J. Gascon, Cryst. *Growth Des.*, 2012, **12**, 3489.

18 O. Shekhah and M. Eddaoudi, *Chem. Commun.*, 2013, **49**, 10079.

19 G. Lu and J. T. Hupp, *J. Am. Chem. Soc.*, 2010, **132**, 7832.

20 W. W. Zhan, Q. Kuang, J. Z. Zhou, X. J. Kong, Z. X. Xie and L. S. Zheng, *J. Am. Chem. Soc.*, 2013, **135**, 1926.

21 J. Q. Jiang, C. X. Yang and X. P. Yan, ACS Appl. Mater., *Interfaces*, 2013, **5**, 9837.

22 J. T. Hughes, D. F. Sava, T. M. Nenoff and A. Navrotsky, *J. Am. Chem. Soc.*, 2013, **135**, 16256.

23 N. A. Khan, B. K. Jung, Z. Hasan and S. H. Jhung, *J. Hazard. Mater.*, 2015, **282**, 194.

24 M. P. Jian, B. Liu, G. S. Zhang, R. P. Liu and X. W. Zhang, *Colloids Surfaces A*, 2015, **465**, 67.

25 B. Russell, J. Villaroel, K. Sapag and A. D. Migone, *J. Phys. Chem. C*, 2014, **118**, 28603.

26 P. A. P. Mendes, A. E. Rodrigues, P. Horcajada, C. Serre and J. A. C. Silva, *Microporous Mesoporous Mater.*, 2014, **194**, 146.

27 M. Zhu, D. Srinivas, S. Bhogeswararao, P. Ratnasamy and M. A. Carreon, *Cataly. Commun.*, 2013, **32**, 36.

28 T. Zhang, , X. F Zhang , X. J. Yan, L. Y. Kong, G. C. Zhang, H. Liu, J. S. Qiu and K. L. Yeung, *Chem. Eng. J.*, 2013, **228**, 398.

29 S. Eslava, L. Zhang, S. Esconjauregui, J. Yang, K. Vanstreels, M. R. Baklanov and E. Saiz, *Chem. Mater.*, 2013, **25**, 27.

30 P. Y. Moh, P. Cubillas, M. W. Anderson and M. P. Attfield, *J. Am. Chem. Soc.*, 2011, **133**, 13304.

31 J. Cravillon, C. A. Schröder, R. Nayuk, J. Gummel, K. Huber and M. Wiebcke, *Angew. Chem.*, 2011, **123**, 8217.

32 Y. Hu, Z. X Liu, J. Xu, Y. N. Huang and Y. Song, *J. Am. Chem. Soc.*, 2013, **135**, 9287.

33 H. Tanaka, S. Ohsaki, S. Hiraide, D. Yamamoto, S. Watanabe and M. T. Miyahara, *J. Phys. Chem. C*, 2014, **118**, 8445.

34 G. Kumari, K. Jayaramulu, T. K. Maji and C. Narayana, *J. Phys. Chem. A*, 2013, **117**, 11006.

35 M. T. Luebbers, T. Wu, L. Shen and R. I. Masel, *Langmuir*, 2010, **26**, 15625.

36 G. Sauerbrey, *Z. Phys.*, 1959,**155**, 206.

37 M. D. Levi, N. Levy, S. Sigalov, G. Salitra, D. Aurbach and J. Maier, *J. Am. Chem. Soc.*, 2010, **132**, 13220.

38 S. Sigalov, M. D. Levi, G. Salitra, D. Aurbach and J. Maier, *Electrochem. Commun.*, 2010, **12**, 1718.

39 S. Z. Yao, *Piezoelectric Chemistry and Biosensors*, 2006, Chemical Industry Press, Beijing.

40 G.N.M. Ferreira, A.C. da-Silva and B. Tomé, *Trends Biotechnol.* ,2009, **27**,689.

41.N. Liu, J.G. Han, Z. Liu, L. J. Qu and Z. X. Gao, *Anal. Methods*, 2013, **5**, 4442.

42 T. Ito, N. Aoki, S. Kaneko and K. Suzuki, *Anal. Methods*, 2014, **6**, 7469

43 X. Huang, J. M. Xu, H. F. Ji, G. F. Lia and H. J. Chen, *Anal. Methods*, 2014, **6**, 4530.

44 L. E. Kreno, K. Leong, O. K. Farha, M. Allendorf, R. P. Van Duyne and J. T. Hupp, *Chem. Rev.*, 2012, **112**, 1105.

45 E. Biemmi, A. Darga, N. Stock and T. Bein, *Microporous Mesoporous Mater.*, 2008, **114**, 380.

46 O. Zybaylo, O. Shekhah, H. Wang, M. Tafipolsky, R. Schmid, D. Johannsmann and C. Wöll, *Phys. Chem. Chem. Phys.*, 2010, **12**, 809.

47 C. Y. Huang, M. Song, Z. Y. Gu, H. F. Wang and X. P. Yan, *Environ. Sci. Technol.*, 2011, **45**, 4490.

48 A. H. Khoshaman and B. Bahreyni, *Sens. Actuators B*, 2012, **162**, 114.

49 A. Bétard, S. Wannapaiboon and R. A. Fischer, *Chem. Commun.*, 2012, **48**, 10493.

50 A. Venkatasubramanian, M. Navaei, K. R. Bagnall, K. C. McCarley, S. Nair and P. J. Hesketh, *J. Phys. Chem. C*, 2012, **116**, 15313.

51 B. Liu, O. Shekhah, H. K. Arslan, J. X. Liu, C. Wöll and R. A. Fischer, *Angew. Chem. Int. Ed.*, 2012, **51**, 807.

52M. Hu, J. Reboul, S. Furukawa, N. L. Torad, Q. Ji, P. Srinivasu, K. Ariga, S. Kitagawa and Y. Yamauchi, *J. Am. Chem. Soc.*, 2012, **134**, 2864.

53 P. Davydovskaya, A. Ranft, B. V. Lotsch and R. Pohle, *Anal. Chem.*, 2014, **86**, 6948.

54 Q. Kang, X.L. Zhu, X.L. Ma, L.Q. Kong, W.T. Xu and D.Z. Shen, *Sens. Actuators B*,2015, **220** ,472.

55 H. Muramatsu, E. Tamiya and I. Karube, *Anal. Chem.*, 1988, **60**, 2142.

56 K K. Kanazawa and J. G Gordon, *Anal. Chim. Acta*, 1985,**175**,99

57 M. Kunze, K. R. Shull and D. Johannsmann, *Langmuir*, 2006, **22**,169

58 S. N. Wijenayake, N. P. Panapitiya, S. H. Versteeg, C. N. Nguyen, S. Goel, K. J. Balkus, Jr., I. H. Musselman and J. P. Ferraris, *Ind. Eng. Chem. Res.*, 2013, **52**, 6991.

59 D. Yamamoto,T. Maki, S. Watanabe, H. Tanaka, M. T. Miyahara and K. Mae, *Chem. Eng. J.* , 2013, **227**, 145.

60 G. McKay and Y. S. Ho, *Process Biochem.*, 1999, **34**, 451.

61 E. Pantatosaki, F. G. Pazzona, G.Megariotis and G. K. Papadopoulos, *J. Phys. Chem. B*,2010, **114**,2493.

62 J.Pérez-Pellitero, H.Amrouche, F. R.Siperstein, G.Pirngruber, C.Nieto-Draghi, G. Chaplais, A.Simon-Masseron, D.Bazer-Bachi, D.Peralta and N. Bats, *Chem. Eur. J.*,2010, **16**,1560.

63 F.Eder and J. A. Lercher, Zeolites,1997,**18**,75.

64 Y. Sağ and T. Kutsal, *Process Biochem.*, 2000, **35**, 801.

65 R. Niwas, U. Gupta, A. A. Khan and K. G. Varshney, *Colloids Surfaces A*, 2010, **164**, 115.

66 V. K. Gupta, P. Singh and N. Rahman, *J. Colloid Interface Sci.*, 2004, **275**, 398.